







RESEARCH ARTICLE | AUGUST 14 2024

Graphitic carbon nitride functionalized with NiO nanoaggregates: An X-ray photoelectron spectroscopy investigation

Special Collection: [Materials for Energy and the Environment](#)

Enrico Scattolin  ; Mattia Benedet  ; Davide Barreca  ; Gian Andrea Rizzi  ; Alberto Gasparotto  ;
Chiara Maccato 



Surf. Sci. Spectra 31, 024001 (2024)

<https://doi.org/10.1116/6.0003732>



Graphitic carbon nitride functionalized with NiO nanoaggregates: An X-ray photoelectron spectroscopy investigation

Cite as: Surf. Sci. Spectra 31, 024001 (2024); doi: 10.1116/6.0003732

Submitted: 3 May 2024 · Accepted: 24 July 2024 ·

Published Online: 14 August 2024



Enrico Scattolin,^{1,a)} Mattia Benedet,^{1,2} Davide Barreca,^{2,b)} Gian Andrea Rizzi,^{1,2} Alberto Gasparotto,^{1,2} and Chiara Maccato^{1,2}

AFFILIATIONS

¹Department of Chemical Sciences, Padova University and INSTM, 35131 Padova, Italy

²CNR-ICMATE and INSTM, Department of Chemical Sciences, Padova University, 35131 Padova, Italy

Note: This paper is part of the 2024 Special Topic Collection on Materials for Energy and the Environment.

^{a)}Electronic mail: enrico.scattolin@studenti.unipd.it

^{b)}Electronic mail: davide.barreca@unipd.it

ABSTRACT

The design and synthesis of low-cost oxygen evolution reaction (OER) photoelectrocatalysts endowed with high activity and durability is of utmost importance for sustainable energy generation *via* solar-assisted water splitting. In this regard, and in the framework of our recent activities, we have focused on the electrophoretic deposition of graphitic carbon nitride (gCN) specimens containing dispersed NiO nanoaggregates on carbon cloth substrates. In the present study, the attention is devoted to the x-ray photoelectron spectroscopy characterization of a representative gCN–NiO specimen. In particular, we provide an analysis of C 1s, N 1s, O 1s, and Ni 2p regions, discussing in detail the main spectral features. The obtained results, that provide evidence for a direct electronic interplay between the single material components, may serve as a useful comparison for additional research on analogous materials for energy and environmental applications.

© 2024 Author(s). All article content, except where otherwise noted, is licensed under a Creative Commons Attribution (CC BY) license (<https://creativecommons.org/licenses/by/4.0/>). <https://doi.org/10.1116/6.0003732>

Accession #: 01955

Technique: XPS

Specimen: gCN–NiO

Instrument: ThermoFisher Scientific Escalab™ QXi

Major Elements in Spectra: C, N, O, and Ni

Minor Elements in Spectra: None

Published Spectra: 5

Spectral Category: Comparison

INTRODUCTION

Over the last two decades, the global population growth and the fast industrial development have produced an ever increasing demand of green and renewable energy (Refs. 1–6). In this context, molecular hydrogen (H₂), featuring a high energy density ($\approx 145 \text{ kJ g}^{-1}$), has emerged as a strategically attractive fuel to tackle the global energetic emergency (Refs. 4 and 7). The required large-scale renewable energy supply can be successfully obtained by means of solar-activated water splitting, possessing an enormous applicative potential thanks to its inherently clean character and the possibility of valorizing natural resources for energy production

(Refs. 1, 4, and 8–10). Nevertheless, an economically viable H₂O-to-H₂ conversion to satisfy the global needs is largely dependent on the availability of efficient (photo)electrocatalysts for the oxygen evolution reaction (OER), the bottleneck of the overall process (Refs. 8 and 11–14).

Among the possible OER photoelectrocatalysts, *n*-type graphitic carbon nitride (gCN) is extremely attractive thanks to its green character, low cost, and favorable physico-chemical properties (Refs. 2, 3, and 15–22). Yet, these advantages are at least partially overwhelmed by the low specific surface area and the high recombination rate of photogenerated electrons and holes, limiting

17 August 2024 15:09:49

the resulting functional performances. Among the numerous research efforts aimed at improving gCN activity (Refs. 5 and 23), over the last years the modulation of the system morphology and the construction of heterojunctions by incorporation of nano-dimensional metal oxides have received a remarkable attention (Refs. 24–27). In particular, the combination of gCN with *p*-type NiO, possessing an appealing stability and reactivity (Refs. 2, 3, 9, and 19), paves the way to interesting research developments for the realization of improved OER photoelectrocatalysts thanks to the synergistic NiO/gCN interfacial interactions (Refs. 9 and 13).

Over the last years, our research group has dedicated an intensive attention to a comparative study and a detailed multitechnique characterization of gCN-based OER electrocatalysts. In particular, we have implemented fast and facile electrophoretic deposition (EPD) routes for the immobilization of gCN-based powders with tailored features on various conducting substrates (Refs. 11, 20, and 24–29). In the present study, gCN–NiO nanocomposites were deposited on carbon cloth (CC) substrates by a single-step EPD route starting from suitably synthesized powder suspensions. A proper modulation of the processing parameters enabled to tailor the content, size distribution, and spatial dispersion of NiO aggregates into the hosting gCN matrix. In the present contribution, a detailed XPS investigation of a representative gCN–NiO nanocomposite specimen is presented, providing a thorough insight into the chemical states of the various elements by the analysis of the main core level peaks (C 1s, N 1s, O 1s, and Ni 2p). A detailed spectral analysis evidenced the formation of gCN/NiO heterojunctions, with an electron flow from NiO to gCN. Such results may act as a pointer for further studies aimed at the design of heterocomposite photoelectrocatalyst materials.

SPECIMEN DESCRIPTION (ACCESSION # 01955)

Specimen: gCN–NiO

CAS Registry #: Unknown

Specimen Characteristics: Homogeneous; solid; polycrystalline; semiconductor; and composite

Chemical Name: Graphitic carbon nitride–nickel(II) oxide

Source: Specimen prepared by EPD on CC, followed by thermal treatment in air at 350 °C for 1 h.

Composition: C, N, O, and Ni

Form: Supported nanocomposite

Structure: X-ray diffraction (XRD) analysis revealed the presence of a broad reflection at $2\theta \approx 25.5^\circ$ ascribed to graphitic carbon in the CC substrate (Ref. 2 and 13), along with a possible gCN contribution. Scanning electron microscopy (SEM) analysis (see the inset in figure accession # 01955-01) evidenced the occurrence of spherical-like gCN aggregates (size range: 1–8 μm) in close contact with nanometer-sized particles comprising cubic NiO as the sole nickel-containing phase, as demonstrated by transmission electron microscopy (TEM) and electron diffraction (ED) results.

History and Significance: gCN powders were synthesized by thermal condensation of a melamine–cyanuric acid adduct following a previously reported route (Ref. 21). The synthesis of NiO-functionalized powders was performed after a careful optimization of a literature procedure (Ref. 14). To this regard,

gCN–NiO powders were prepared by adding $\text{Ni}(\text{OAc})_2 \cdot 4\text{H}_2\text{O}$ (0.03 mol) to a suspension of gCN in de-ionized water (0.1 g in 75 ml) maintained under stirring. After sonication for 2 h and complete solvent evaporation by gentle heating, the collected brownish powders were annealed in air at 300 °C for 30 min (heating rate = 3 °C/min).

CC substrates ($\approx 1 \times 0.8 \text{ cm}^2$; E35, Quintech; area weight: 164 g/m²) were subjected to a precleaning procedure consisting of sonication in de-ionized water, isopropyl alcohol, and acetone. Immobilization of gCN–NiO on CC was performed by EPD, starting from a suspension of 40 mg of the above gCN–NiO powders and 10 mg of I₂ in acetone (50 ml), applying a constant potential difference of 10 V (deposition time = 60 s). A graphite stripe was used as counterelectrode. The obtained sample was finally subjected to thermal treatment in air at 350 °C for 60 min (heating rate = 3 °C/min).

As Received Condition: As-grown

Analyzed Region: Same as the host material

Ex Situ Preparation/Mounting: The specimen was fixed on a grounded sample holder by metallic clips and introduced into the analysis chamber through a fast entry system.

In Situ Preparation: The specimen was analyzed as-received.

Charge Control: Charge compensation was performed by a dual-beam low energy electron and ion coaxial flood source (0.1 V, 175 μA , and gas cell at 20 V).

Temp. During Analysis: 298 K

Pressure During Analysis: $<10^{-8}$ Pa

Preanalysis Beam Exposure: 130 s

INSTRUMENT DESCRIPTION

Manufacturer and Model: ThermoFisher Scientific EscalabTM QXi

Analyzer Type: Spherical sector

Detector: Channeltron

Number of Detector Elements: 6

INSTRUMENT PARAMETERS COMMON TO ALL SPECTRA

Spectrometer

Analyzer Mode: Constant pass energy

Throughput ($T = E^N$): The transmission function is calculated from a cubic polynomial fit to a plot of $\log[\text{peak area}/(\text{PE} \times \text{XSF})]$ versus $\log(\text{KE}/\text{PE})$, where PE is the pass energy, KE is the kinetic energy, and XSF is the relative sensitivity factor (Ref. 24).

Excitation Source Window: None

Excitation Source: Al K_α monochromatic

Source Energy: 1486.6 eV

Source Strength: 200 W

Source Beam Size: $500 \times 500 \mu\text{m}^2$

Signal Mode: Single channel direct

Geometry

Incident Angle: 58°

Source-to-Analyzer Angle: 58°

Emission Angle: 0°
Specimen Azimuthal Angle: 90°
Acceptance Angle from Analyzer Axis: 45°
Analyzer Angular Acceptance Width: 22.5° × 22.5°

Ion Gun

Manufacturer and Model: ThermoFisher Scientific MAGCIS Dual Beam Ion Source
Energy: 4000 eV
Current: 7 mA
Current Measurement Method: Biased stage
Sputtering Species and Charge: Ar⁺
Spot Size (unrastered): 500 μm
Raster Size: 4500 × 4500 μm²
Incident Angle: 40°
Polar Angle: 40°
Azimuthal Angle: 270°
Comment: Differentially pumped ion gun

DATA ANALYSIS METHOD

Energy Scale Correction: The reported binding energies were corrected for charging phenomena by assigning a BE of 284.8 eV to the adventitious C 1s signal (Ref. 30). In principle, due to the complex C 1s spectral shape, charge referencing may apparently possess a relatively large uncertainty (±0.2 eV). Nevertheless, the validity of the presently reported results is supported by a detailed comparison of the contributing band positions with previous literature results on homologous systems (Refs. 20, 24, and 25).

Recommended Energy Scale Shift: +1.46 eV

Peak Shape and Background Method: After performing a Shirley-type background subtraction (Ref. 31), least-squares fitting was performed adopting Gaussian/Lorentzian sum functions.

Quantitation Method: Atomic concentrations were calculated by peak area integration, using sensitivity factors provided by Thermo Scientific Avantage software (version 6.6.0).

ACKNOWLEDGMENTS

The authors acknowledge financial support from CNR (Progetti di Ricerca @CNR—avviso 2020—ASSIST), Padova University (P-DiSC#04BIRD2020-UNIPD EUREKA, P-DiSC#02BIRD2023-UNIPD RIGENERA, DOR 2021–2023), INSTM Consortium (INSTM21PD GASPAROTTO-NANOMAT and INSTM21PDBARMAC-ATENA), and PRIN 2022474YE8 (SCI-TROPHY project), finanziato dall'Unione Europea - Next Generation EU - Bando PRIN 2022 – M4.C2.1.1. The instrument used in this study was funded by “Sviluppo delle infrastrutture e programma biennale degli interventi del Consiglio Nazionale delle Ricerche (2019).”

AUTHOR DECLARATIONS

Conflict of Interest

The authors have no conflicts to disclose.

Author Contributions

Enrico Scattolin: Investigation (lead); Software (equal); Validation (equal); Writing – review & editing (equal). **Mattia Benedet:** Data curation (equal); Methodology (equal); Validation (equal); Visualization (equal). **Davide Barreca:** Conceptualization (lead); Formal analysis (lead); Funding acquisition (lead); Supervision (equal); Writing – review & editing (lead). **Gian Andrea Rizzi:** Data curation (equal); Funding acquisition (equal); Investigation (equal); Writing – review & editing (equal). **Alberto Gasparotto:** Data curation (lead); Formal analysis (lead); Funding acquisition (equal); Investigation (equal); Methodology (equal); Writing – original draft (lead). **Chiara Maccato:** Formal analysis (equal); Funding acquisition (lead); Methodology (equal); Supervision (equal); Visualization (equal); Writing – review & editing (equal).

DATA AVAILABILITY

The data that support the findings of this study are available within the article and its [supplementary material](#).

REFERENCES

- 1 H. Yang, H. Guo, K. Pang, P. Fan, X. Li, W. Ren, and R. Song, *Nanoscale* **12**, 7024 (2020).
- 2 W. Wang, B. Lv, and F. Tao, *Environ. Sci. Pollut. Res.* **30**, 25620 (2023).
- 3 L. Wang, Y. Dong, J. Zhang, F. Tao, and J. Xu, *J. Solid State Chem.* **308**, 122878 (2022).
- 4 L. Wang, W. Si, Y. Tong, F. Hou, D. Pergolesi, J. Hou, T. Lippert, S. X. Dou, and J. Liang, *Carbon Energy* **2**, 223 (2020).
- 5 L. Wang, Y. Li, X. Yin, Y. Wang, A. Song, Z. Ma, X. Qin, and G. Shao, *ACS Sustainable Chem. Eng.* **5**, 7993 (2017).
- 6 X. Li, H. Zhang, Y. Liu, X. Duan, X. Xu, S. Liu, H. Sun, and S. Wang, *Chem. Eng. J.* **390**, 124634 (2020).
- 7 D. Guo, Z. Zhao, M.-Y. Zong, C. Fan, W. Zheng, and D. Wang, *ACS Sustainable Chem. Eng.* **11**, 8362 (2023).
- 8 K. Hemmati, A. Kumar, A. R. Jadhav, O. Moradlou, A. Z. Moshfegh, and H. Lee, *ACS Catal.* **13**, 5516 (2023).
- 9 S. Noor, R. S. Haider, S. Noor, S. Sajjad, S. A. Khan Leghari, M. Mehboob, and M. Long, *Int. J. Hydrogen Energy* **47**, 36517 (2022).
- 10 S. Zhang, J. Yan, S. Yang, Y. Xu, X. Cai, X. Li, X. Zhang, F. Peng, and Y. Fang, *Chin. J. Catal.* **38**, 365 (2017).
- 11 M. Benedet *et al.*, *J. Mater. Chem. A* **11**, 21595 (2023).
- 12 P. Chaudhary and P. P. Ingole, *Int. J. Hydrogen Energy* **45**, 16060 (2020).
- 13 C. Liao *et al.*, *Adv. Funct. Mater.* **29**, 1904020 (2019).
- 14 M. I. Chebanenko, A. A. Lobinsky, V. N. Nevedomskiy, and V. I. Popkov, *Dalton Trans.* **49**, 12088 (2020).
- 15 J. Liu, Q. Jia, J. Long, X. Wang, Z. Gao, and Q. Gu, *Appl. Catal. B* **222**, 35 (2018).
- 16 Y. Fu *et al.*, *Inorg. Chem. Front.* **5**, 1646 (2018).
- 17 P. Qiu, C. Xu, H. Chen, F. Jiang, X. Wang, R. Lu, and X. Zhang, *Appl. Catal. B* **206**, 319 (2017).
- 18 T. Zhang, P. Liu, L. Wang, S. Wang, J. Shi, and X. Lan, *Materials* **14**, 2894 (2021).
- 19 J. Tang, R. Guo, W. Zhou, C. Huang, and W. Pan, *Appl. Catal. B* **237**, 802 (2018).
- 20 M. Benedet, A. Gasparotto, G. A. Rizzi, D. Barreca, and C. Maccato, *Surf. Sci. Spectra* **29**, 024001 (2022).
- 21 Y.-S. Jun, E. Z. Lee, X. Wang, W. H. Hong, G. D. Stucky, and A. Thomas, *Adv. Funct. Mater.* **23**, 3661 (2013).
- 22 L. Lei, W. Wang, C. Wang, M. Zhang, Q. Zhong, and H. Fan, *Ceram. Int.* **47**, 1258 (2021).
- 23 Z. Zhao, Y. Sun, and F. Dong, *Nanoscale* **7**, 15 (2015).
- 24 M. Benedet, A. Gasparotto, G. A. Rizzi, C. Maccato, D. Mariotti, R. McGlynn, and D. Barreca, *Surf. Sci. Spectra* **30**, 024018 (2023).

- ²⁵M. Benedet, G. A. Rizzi, D. Barreca, A. Gasparotto, and C. Maccato, *Surf. Sci. Spectra* **30**, 014004 (2023).
- ²⁶M. Benedet, G. A. Rizzi, A. Gasparotto, N. Gauquelin, A. Orekhov, J. Verbeeck, C. Maccato, and D. Barreca, *Appl. Surf. Sci.* **618**, 156652 (2023).
- ²⁷S. Benedoue *et al.*, *Nanomaterials* **13**, 1035 (2023).
- ²⁸M. Benedet *et al.*, *ACS Appl. Mater. Interfaces* **15**, 47368 (2023).
- ²⁹M. Benedet, G. A. Rizzi, A. Gasparotto, O. I. Lebedev, L. Girardi, C. Maccato, and D. Barreca, *Chem. Eng. J.* **448**, 137645 (2022).
- ³⁰D. Briggs and M. P. Seah, *Practical Surface Analysis: Auger and X-ray Photoelectron Spectroscopy*, 2nd ed. (Wiley, New York, 1990).
- ³¹D. A. Shirley, *Phys. Rev. B* **5**, 4709 (1972).
- ³²I. Bertóti, M. Mohai, and K. László, *Carbon* **84**, 185 (2015).
- ³³X. Li, Y. Wang, W. Tian, and J. Cao, *ACS Omega* **4**, 9645 (2019).
- ³⁴P. Qiu, H. Chen, and F. Jiang, *RSC Adv.* **4**, 39969 (2014).
- ³⁵M. A. Peck and M. A. Langell, *Chem. Mater.* **24**, 4483 (2012).
- ³⁶O. Pérez, O. F. Odio, and E. Reguera, *New J. Chem.* **46**, 11255 (2022).
- ³⁷T. Haq and Y. Haik, *ACS Sustainable Chem. Eng.* **10**, 6622 (2022).
- ³⁸D. Alders, F. C. Voogt, T. Hibma, and G. A. Sawatzky, *Phys. Rev. B* **54**, 7716 (1996).
- ³⁹I. Preda, R. J. O. Mossaneck, M. Abbate, L. Alvarez, J. Méndez, A. Gutiérrez, and L. Soriano, *Surf. Sci.* **606**, 1426 (2012).
- ⁴⁰G. Pagot, M. Benedet, C. Maccato, D. Barreca, and V. Di Noto, *Surf. Sci. Spectra* **30**, 024028 (2023).
- ⁴¹M. Benedet *et al.*, *J. Phys. Chem. C* **127**, 22304 (2023).
- ⁴²Y. Li *et al.*, *Chem. Sci.* **12**, 3633 (2021).
- ⁴³K. Qi, A. Zada, Y. Yang, Q. Chen, and A. Khataee, *Res. Chem. Intermed.* **46**, 5281 (2020).
- ⁴⁴J. Zhang, J. Wang, Y. Fu, B. Zhang, and Z. Xie, *J. Mater. Chem. C* **2**, 8295 (2014).

SPECTRAL FEATURES TABLE

Spectrum ID #	Element/Transition	Peak Energy (eV)	Peak Width FWHM (eV)	Peak Area (eV × counts/s)	Sensitivity Factor	Concentration (at. %)	Peak Assignment
01955-02 ^a	C 1s	284.8	1.8	2 431.8	1.000	2.2	Adventitious contamination and C—C bonds in the CC substrate
01955-02 ^a	C 1s	285.8	2.1	5 752.1	1.000	5.2	C in C—NH _x (x = 1 and 2) groups on gCN edges, C—O bonds of gCN with NiO
01955-02 ^a	C 1s	288.1	1.6	22 821.5	1.000	20.4	N=C—N carbon atoms in gCN aromatic rings; carbonyl groups from the CC substrate
01955-02 ^a	C 1s	289.2	2.1	14 216.7	1.000	12.7	Carboxylate/esters group from the CC substrate
01955-02 ^a	C 1s	293.8	2.2	1 543.3	1.000	1.4	Excitation of π-electrons
01955-03 ^b	N 1s	398.4	1.5	41 052.6	1.676	21.9	Two-coordinated C=N—C nitrogen atoms from gCN
01955-03 ^b	N 1s	399.6	1.7	29 677.6	1.676	15.9	Tertiary N—(C) ₃ nitrogen atoms from gCN
01955-03 ^b	N 1s	401.0	1.9	12 144.7	1.676	6.5	Uncondensed NH _x groups
01955-03 ^b	N 1s	404.0	2.8	2 651.3	1.676	1.4	Excitation of π-electrons
01955-04 ^c	O 1s	530.3	2.0	9 030.9	2.881	2.9	Lattice oxygen in NiO
01955-04 ^c	O 1s	531.6	1.9	16 956.9	2.881	5.4	Surface adsorbed hydroxyl groups; carbonyl/carboxylate/esters groups from the CC substrate
01955-04 ^c	O 1s	533.1	1.9	2 999.3	2.881	1.0	Adsorbed H ₂ O; C—O—Ni bonds
01955-05 ^d	Ni 2p	71 615.9	20.765	3.1	Ni(II) in NiO
01955-05 ^d	Ni 2p _{3/2}	855.5	(a) Ni 2p _{3/2}
01955-05 ^d	Ni 2p _{3/2}	861.2	(b) Ni 2p _{3/2}
01955-05 ^d	Ni 2p _{1/2}	873.3	(c) Ni 2p _{1/2}
01955-05 ^d	Ni 2p _{1/2}	879.5	(d) Ni 2p _{1/2}

^aThe sensitivity factor is referred to the whole C 1s signal.

^bThe sensitivity factor is referred to the whole N 1s signal.

^cThe sensitivity factor is referred to the whole O 1s signal.

^dThe sensitivity factor, peak area, and concentration are referred to the whole Ni 2p signal.

Footnote to Spectrum 01955-01: The wide-scan spectrum revealed the presence of carbon, nitrogen, oxygen, and nickel photoelectron and Auger signals, whose occurrence confirmed the copresence of gCN and NiO, in line with the spectral features discussed below.

Footnote to Spectrum 01955-02: A visual inspection of the C 1s peak displays the clear evidence of at least four peaks: a shoulder on the low BE side, two different contributions to the most intense central signal (showing a tailing on the high BE side), and a minor high BE peak. Nevertheless, a more detailed analysis highlights the concurrence of two different contributions to the low BE feature, accounting, thus, for five contributing components.

The first band, centered at 284.8 eV, was attributed to adventitious carbon contamination due to air exposure/manipulation (Refs. 24 and 25) and contained also an overlapped contribution due to C—C bonds from the carbon cloth substrate (Refs. 19 and 32), indicating its incomplete coverage. The signal at 285.8 eV was ascribed to C in C—NH_x (x = 1 and 2) groups on gCN edges, deriving from an incomplete condensation (Refs. 11, 26, 27, and 33), and even to C—O bonds between gCN and NiO (Refs. 2, 6, and 17). The latter can facilitate a direct electronic interplay between the system components, favorably affecting the ultimate functional performances (Ref. 24). The main peak, centered at 288.1 eV, was correlated with carbon atoms belonging to N=C—N in gCN aromatic rings (Refs. 18–20, 25–27, and 29) and contained also the contribution from carbonyl groups of the carbon cloth (Ref. 32). The latter was also responsible for the presence of carboxylate and ester groups, generating the band at 289.2 eV (Ref. 32). The last minor peak, located at 293.8 eV, was assigned to π-electron excitations (Refs. 17 and 34).

Footnote to Spectrum 01955-03: The occurrence of graphitic carbon nitride in the analyzed system was unambiguously confirmed by the N 1s photoelectron peak features, that were perfectly in line with those of our recent publications on gCN-containing systems (Refs. 20, 24, 26, and 29). In particular, the main N 1s contributing band, located at 398.4 eV, was assigned to two-coordinated C=N—C nitrogen atoms in gCN, whereas the peak at 399.6 eV was correlated with tertiary N—(C)₃ nitrogen atoms in heptazine carbon nitride rings. The signal at 401.0 eV was attributed to NH_x (x = 1 and 2) moieties, and the peak located at 404.0 eV was due to excitation of π-electrons in gCN heptazine rings (Refs. 1, 3, 6, 15–18, 20, 28, and 33).

It is worthy observing that the actual energy positions of C 1s and N 1s bands underwent a blue shift in comparison to bare gCN (Refs. 25 and 26). This result, along with an opposite BE shift of NiO O 1s and Ni 2p spectral components (see below), suggested the formation of a p-n heterojunction at the NiO/gCN interface (Refs. 2 and 15). Correspondingly, photogenerated electrons and holes are accumulated in the gCN conduction band and the NiO valence band, respectively, suppressing detrimental recombination processes and paving the way to an improved system photoactivity.

17 August 2024 15:09:49

SPECTRAL FEATURES TABLE. (Continued.)

Footnote to Spectrum 01955-04: Fitting of the O 1s photopeak was performed with three contributing bands. A first component at 530.3 eV, ascribed to lattice oxygen in Ni(II) oxide (Refs. 6, 8, 16, and 35). The component centered at 531.6 eV was attributed to surface chemisorbed hydroxyl groups (Refs. 12, 19, 27, 28, and 35) and to carboxylate/ester groups from the CC substrate (Ref. 36) and contained even a contribution from CC carbonyl groups (Ref. 32). The last peak at 533.1 eV was ascribed to surface adsorbed water (Refs. 17 and 37), and to C—O—Ni bonds between NiO and gCN (Refs. 6 and 28), in line with the above discussed C 1s spectral features. The present BE for the lattice O band was shifted to higher BEs in comparison to bare NiO (Refs. 8, 16, and 38), confirming, thus, the occurrence of the aforementioned heterojunctions and the related charge transfer mechanism.

Footnote to Spectrum 01955-05: The Ni 2p signal was characterized by a peculiar multiplet structure, more complex than the classical doublet expected for a simple spin-orbit separation. The particular spectral shape is directly dependent on the Ni local environment and is very sensitive to material crystallinity and defectivity. In particular, the features can significantly depend on surface contribution for low substrate coverages and/or highly dispersed NiO systems, as in the present case (Refs. 6, 38, and 39).

As a matter of fact, the correct assignment of Ni 2p peak features has been the subject of debate, and controversial explanations are available in the literature. The interpretation of Ni 2p spectral features can be proposed as follows. NiO is a charge transfer oxide in which the ground state is a mixture of $3d^8$, $3d^8\bar{O}$, and $3d^{10}\bar{O}^2$ configurations, where \bar{O} denotes a hole at the Ni-coordinated oxygen site. A similar electronic structure is responsible for the presence of the observed multiplet, which has been widely discussed in the literature (Refs. 39–41). Nowadays, as regards the $j = 3/2$ spin-orbit component features [labeled as (a) and (b) in the Spectral Features Table], it is commonly accepted that (a) corresponds to the $\bar{c}3d^8\bar{O}$ configuration (where \bar{c} denotes a Ni 2p core level hole), whereas (b) is related to $3d^{10}\bar{O}^2$ and $\bar{c}3d^8$ ones.

Nevertheless, in various works, Ni(III) contents comparable (or even higher) than Ni(II) ones, or the copresence of Ni₂O₃ and NiO, have been claimed basing on the sole XPS analyses. As a matter of fact, such an interpretation is in contrast with the occurrence of the same spectral features even for NiO single crystals freshly cleaved in vacuum, indicating that the observed Ni 2p structure is unique to NiO. Hence, the presence of Ni₂O₃ in such cases has to be excluded (Ref. 40). The absence of signals at 853.2 and 852.7 eV confirmed the lack of Ni(0) and Ni nitride in appreciable quantities (Refs. 12, 13, 18, and 42).

A comparison with the literature on NiO nanostructures and NiO—gCN nanocomposites (Refs. 6, 16, 35, 39, and 43) reveals a direct analogy of the present Ni 2p features with previous reports, in accordance with the dispersion of nanometer-sized NiO aggregates into the hosting gCN matrix. The above observations are corroborated by TEM and ED analyses, which highlighted the presence of NiO as the only nickel-containing phase (see also the “Structure” section), ruling out the occurrence of Ni(OH)₂.

On the other hand, the present Ni 2p BE values underwent an upward shift in comparison to the values reported for bare NiO (Refs. 38, 39, and 44). As already mentioned, such a phenomenon could be explained basing on the formation of NiO/gCN heterojunctions, with a NiO → gCN electron transfer paving the way to an enhanced photocarrier separation, promoted by the intimate graphitic carbon nitride/nickel(II) oxide contact and the occurrence of C—O—Ni bonds in the target materials.

ANALYZER CALIBRATION TABLE

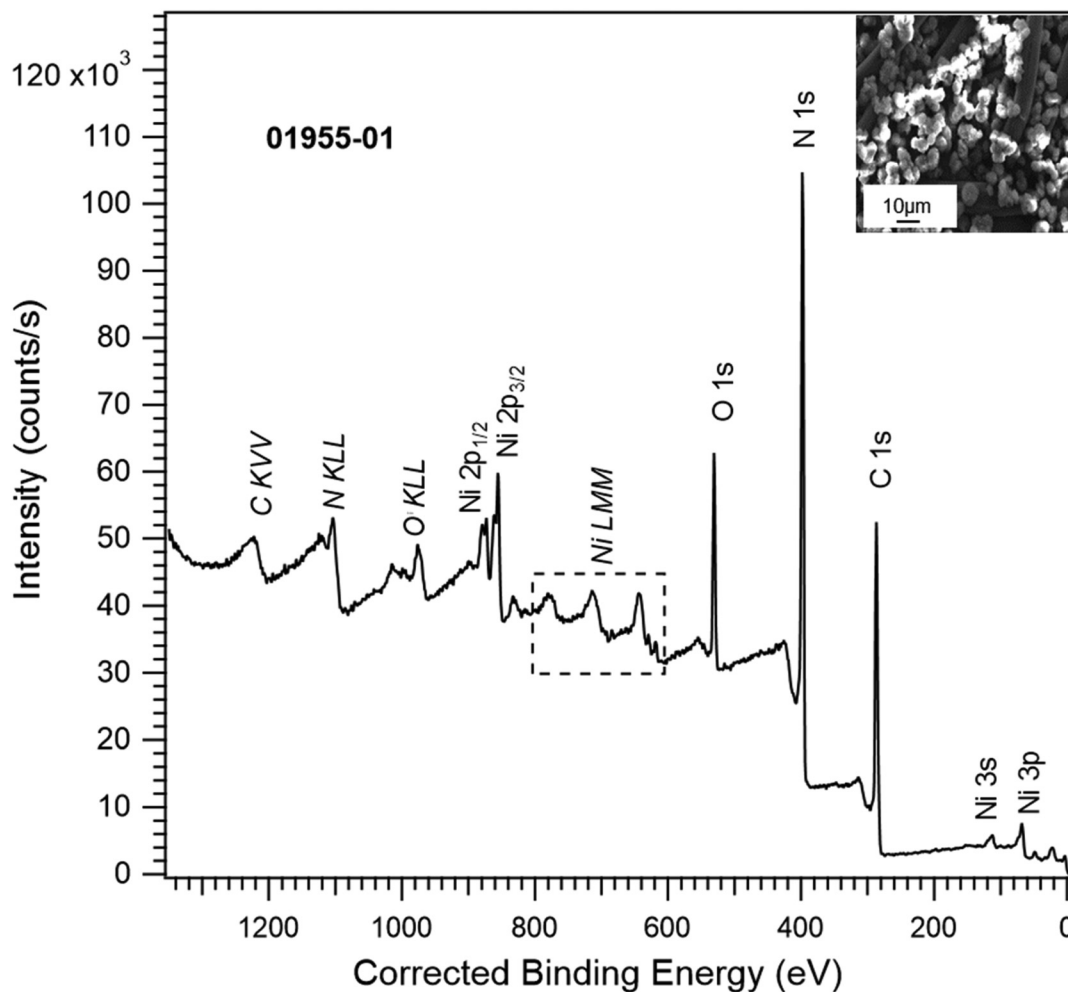
Spectrum ID #	Element/Transition	Peak Energy (eV)	Peak Width FWHM (eV)	Peak Area (eV × counts/s)	Sensitivity Factor	Concentration (at. %)	Peak Assignment
...	Au 4f _{7/2}	84.0	1.1	2 841 305.7	20.735	...	Au(0)
...	Cu 2p _{3/2}	932.7	1.3	5 350 621.8	26.513	...	Cu(0)

Comment to Analyzer Calibration Table: The peaks were acquired after Ar⁺ erosion.

GUIDE TO FIGURES

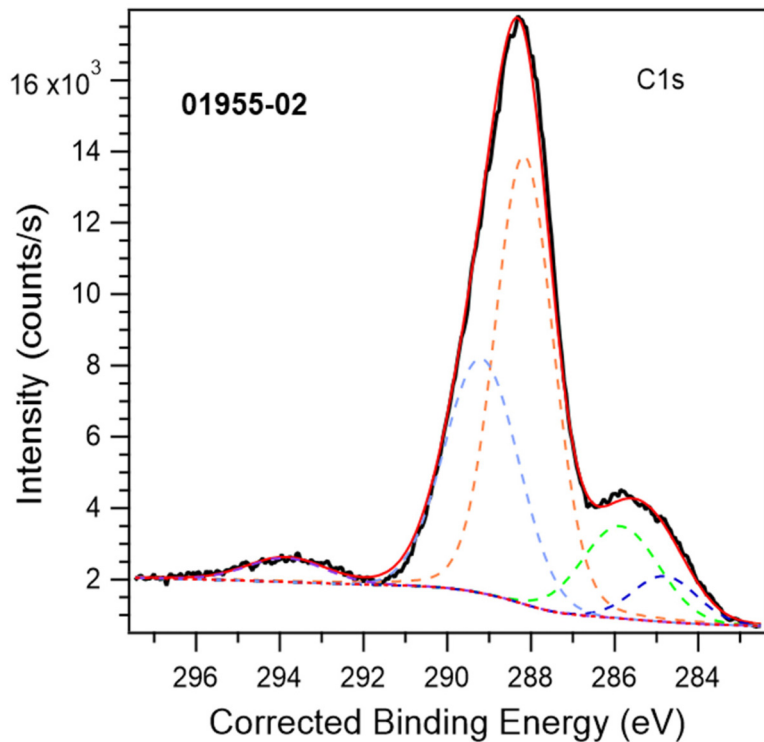
Spectrum (Accession) #	Spectral Region	Voltage Shift ^a	Multiplier	Baseline	Comment #
01955-01	Survey	−1.46	1	0	...
01955-02	C 1s	−1.46	1	0	...
01955-03	N 1s	−1.46	1	0	...
01955-04	O 1s	−1.46	1	0	...
01955-05	Ni 2p	−1.46	1	0	...

^aVoltage shift of the archived (as-measured) spectrum relative to the printed figure. The figure reflects the recommended energy scale correction due to a calibration correction, sample charging, flood gun, or other phenomenon.



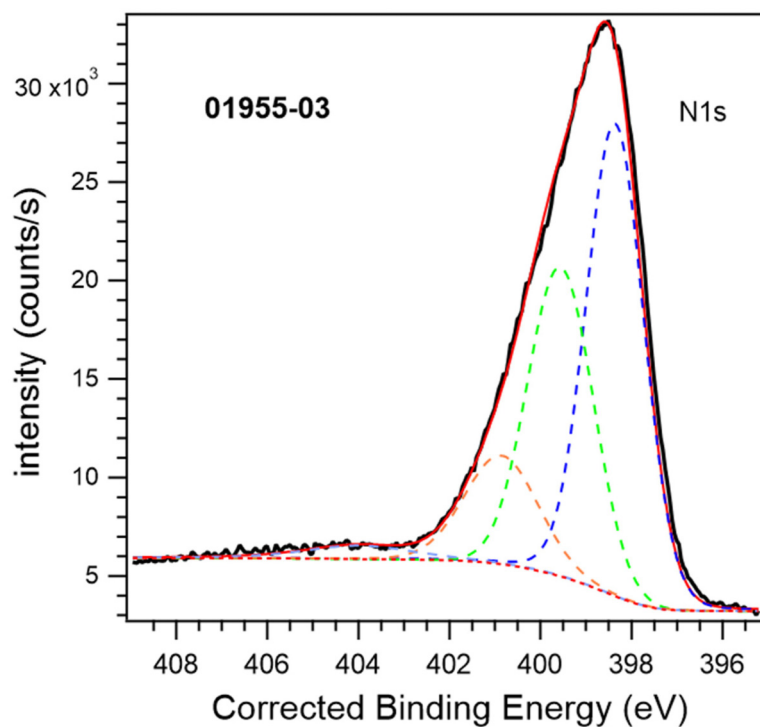
17 August 2024 15:09:49

Accession #:	01955-01
Specimen:	gCN-NiO
Technique:	XPS
Spectral Region:	Survey
Instrument:	ThermoFisher Scientific Escalab™ QXi
Excitation Source:	Al K _α monochromatic
Source Energy:	1486.6 eV
Source Strength:	200 W
Source Size:	0.50 × 0.50 mm ²
Analyzer Type:	Spherical sector analyzer
Incident Angle:	58°
Emission Angle:	0°
Analyzer Pass Energy:	150 eV
Analyzer Resolution:	1.5 eV
Total Signal Accumulation Time:	408.3 s
Total Elapsed Time:	449.1 s
Number of Scans:	6
Effective Detector Width:	1.5 eV



■ **Accession #:** [01955-02](#)
 ■ **Specimen:** gCN-NiO
 ■ **Technique:** XPS
 ■ **Spectral Region:** C 1s

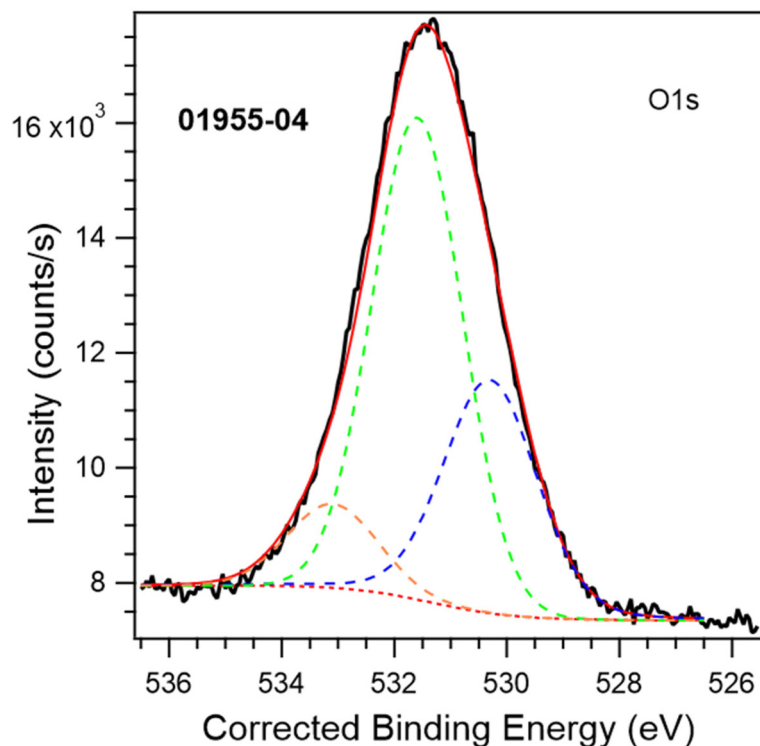
Instrument: ThermoFisher Scientific EscalabTM QXi
 Excitation Source: Al K_{α} monochromatic
 Source Energy: 1486.6 eV
 Source Strength: 200 W
 Source Size: 0.50 × 0.50 mm²
 Analyzer Type: Spherical sector
 Incident Angle: 58°
 Emission Angle: 0°
 Analyzer Pass Energy: 50 eV
 Analyzer Resolution: 0.5 eV
 Total Signal Accumulation Time: 114.3 s
 Total Elapsed Time: 125.7 s
 Number of Scans: 6
 Effective Detector Width: 0.5 eV



■ **Accession #:** [01955-03](#)
 ■ **Specimen:** gCN-NiO
 ■ **Technique:** XPS
 ■ **Spectral Region:** N 1s

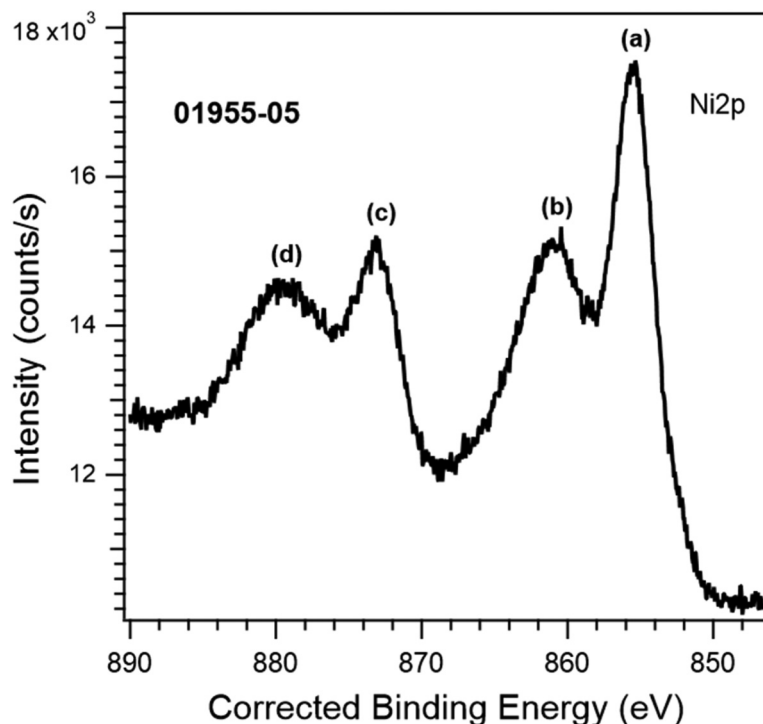
Instrument: ThermoFisher Scientific EscalabTM QXi
 Excitation Source: Al K_{α} monochromatic
 Source Energy: 1486.6 eV
 Source Strength: 200 W
 Source Size: 0.50 × 0.50 mm²
 Analyzer Type: Spherical sector
 Incident Angle: 58°
 Emission Angle: 0°
 Analyzer Pass Energy: 50 eV
 Analyzer Resolution: 0.5 eV
 Total Signal Accumulation Time: 90.3 s
 Total Elapsed Time: 99.3 s
 Number of Scans: 5
 Effective Detector Width: 0.5 eV

17 August 2024 15:09:49



■ **Accession #:** 01955-04
 ■ **Specimen:** gCN-NiO
 ■ **Technique:** XPS
 ■ **Spectral Region:** O 1s

Instrument: ThermoFisher Scientific EscalabTM QXi
 Excitation Source: Al K_{α} monochromatic
 Source Energy: 1486.6 eV
 Source Strength: 200 W
 Source Size: 0.50 × 0.50 mm²
 Analyzer Type: Spherical sector
 Incident Angle: 58°
 Emission Angle: 0°
 Analyzer Pass Energy: 50 eV
 Analyzer Resolution: 0.5 eV
 Total Signal Accumulation Time: 240.6 s
 Total Elapsed Time: 264.7 s
 Number of Scans: 12
 Effective Detector Width: 0.5 eV



■ **Accession #:** 01955-05
 ■ **Specimen:** gCN-NiO
 ■ **Technique:** XPS
 ■ **Spectral Region:** Ni 2p

Instrument: ThermoFisher Scientific EscalabTM QXi
 Excitation Source: Al K_{α} monochromatic
 Source Energy: 1486.6 eV
 Source Strength: 200 W
 Source Size: 0.50 × 0.50 mm²
 Analyzer Type: Spherical sector
 Incident Angle: 58°
 Emission Angle: 0°
 Analyzer Pass Energy 50 eV
 Analyzer Resolution: 0.5 eV
 Total Signal Accumulation Time: 961.0 s
 Total Elapsed Time: 1057.1 s
 Number of Scans: 20
 Effective Detector Width: 0.5 eV

17 August 2024 15:09:49